Journal of Theoretical and Applied Vibration and Acoustics 9 (1) 1-13 (2023)

I S A V

Journal of Theoretical and Applied

Vibration and Acoustics

journal homepage: http://tava.isav.ir

Modeling and identification of nonlinear behavior of friction vibratory separators using Iwan model

Majid Rajaei [a,*], **Hamid Ahmadian** [b], **Ehsan Tavakoli** [c]

[a] *Assistant Professor, School of Mechanical Engineering, Arak University of Technology, Arak, IRAN*

[b] *Professor, School of Mechanical Engineering, Iran University of Science and Technology, Tehran, IRAN*

[c] *Ph.D. Candidate, School of Mechanical Engineering, Iran University of Science and Technology, Tehran, IRAN*

ARTICLE INFO

Article history:
Received 30 February 2022

Received in revised form
5 April 2023

Accepted 30 June 2023

Available online 14 July 2023

Keywords:
Microslip,

Iwan model,

Vibration,

Separator,

Hysteresis loop.

ABSTRACT

In some friction vibratory separators, the variations in the vertical forces and slip speed affect the damping rate and behavior of microslip and macroslip friction forces, leading to asymmetry in the force-displacement hysteresis loop diagram. High flexibility in modeling hysteresis loops and physical interpreting of their parameters is the advantage of the Iwan model. However, the effects of slip speed and changing vertical forces on the friction surfaces have not been included in the model. The present study aims to develop the generalized Iwan model by including the effects of slip speed and changing vertical forces on the friction surfaces for modeling the vibratory behavior of friction separators with asymmetric hysteresis. In the experimental set-up, a friction separator made by passing a compressed polymer rope through a spring is subjected to identification tests at different stimulation frequencies and amplitudes. Finally, the generalized Iwan model is updated to match its output with the results from tests using the genetic algorithm by optimizing the parameters.

1. Introduction

The passive separator is usually used to improve the efficiency of the equipment sensitive to vibration and shock, leading to a significant reduction in annoying vibrations transmitted to equipment by establishing flexibility and proper depreciation. Therefore, it is necessary to define and verify the mathematical model of vibratory separator responses to input stimuli for the

* Corresponding author:
E-mail address: m.rajaei@arakut.ac.ir (M.Rajaei)

http://dx.doi.org/10.22064/tava.2023.1973376.1221

optimal design of the separators and to model their behavior and effect on the equipment performance.

The friction passive separators are the most effective separators that perform better in high-speed vibratory stimulation because of approximately stable friction forces at different slip speeds, and they do not suffer from stiffness, unlike viscous dampers. In the present study, the friction separator consists of the extension springs through which a compressed polymer rope is passed.

The passive separator well reduces the vibration amplitudes whose frequency is greater than twice the separator's natural frequency. Thus, the softer the separator, the less its natural frequency with a highly effective performance frequency range. However, the softer separators lead to increased displacements against shocks, low-frequency vibrations, and exerted forces such as weight, which is not desirable. This problem, the maximum separator displacement in different directions, can be solved (limited) by adjusting the length of the rope passed through the springs.

The behavior of the separator force relative to displacement is nonlinear due to the nonlinear nature of friction force which includes microslip, macroslip and slip-stick phenomenon. Also, it is predictable that the vertical force on the frictional contact surface differs during the longitudinal oscillation of the springs due to spring geometry and compressed polymer rope between their rings with variable distances from each other.

The force-displacement hysteresis loop diagram is achieved in an oscillating round-trip path of the vibratory separator. To model the separator behavior, it is necessary to identify the mathematical model of the hysteresis loop at different oscillation amplitudes and frequencies to predict the behavior of the vibratory separator force. To date, different methods have been developed for modeling the friction-induced hysteresis loop.

Iwan [1-3] has presented a physical model for modeling the nonlinear hysteresis behavior in the structures and materials using the Jenkins spring-slider elements connected in parallel. Bouc [3] has also presented a model using a first-order differential equation to analyze the nonlinear random vibrations. Wen [4] generalized the Bouc model as a novel one called the Bouc-Wen model to model ideal elastoplastic behavior. Schwanen and Nijmeijer [5] used the generalized Bouc-Wen model to describe the vibratory and hysteresis behaviors of a cable separator subjected to quasi-static cyclic loading. They found that this model is unable to model well the dynamic separator responses at small oscillation amplitudes. Rashidi [6], Leblouba [7], and some other researchers [8-10] used the generalized Bouc-Wen model with different improvements to model the force of the hysteresis loop in the nonlinear cable separators. Jeffrey and Shan Hsu [11] achieved the hysteresis curves for some different examples using the Tinker and Bouc-Wen models and found that the nonlinear hysteresis behaviors of spiral cable separators can be predicted using these mathematical models.

Although the Bouc-Wen model has a good ability to model the hysteresis loops, not all of its parameters can be interpreted physically, and in fact, it is a quasi-physical model. However, the Iwan model includes parameters with full physical interpretation, which is an important advantage in understanding the nature of the friction phenomenon. Rajaei and Ahmadian [12, 13] included the effect of normal force on the friction force in the Iwan model by generalizing the model and presented a method to determine its distribution function for friction connections based on the time domain data.

The present study tries to develop the Iwan model for simulating the speed-dependent asymmetric force-displacement hysteresis loops observed in some problems such as friction separators with variable vertical forces.

Numerous studies have been conducted on the friction behavior between steel and polymer surfaces. For example, Mens and Gee [14] investigated the friction and wear behavior of 18 different polymers in contact with steel at different temperatures and concluded that the addition of PTFE to PA66 polymer leads to a reduced coefficient of friction to less than 0.2 and reduced wear. Myshkin et al. [15] investigated the studies conducted on the friction, adhesion, and wear of polymers concentrating on the effect of temperature, vertical pressure, and slip speed on the friction rate on the contact surface. Rodriguez et al. [16] conducted a study on the friction and wear of Polyamide 6 (PA6) and Polyamide 6.6 (PA6.6), emphasizing the excellent properties of the polyamide in mechanical strength and wear resistance. Nuruzzaman and Chowdhury [17] addressed the determination of the coefficient of friction between stainless steel in contact with different polymers and composites in different loadings and slip speeds. They found that the coefficient of friction increases by increasing the vertical force and slip speed in all tested polymers except PA66.

In the present research, in the first section, the experimental model is introduced and the identification tests are performed for a rope spring separator sample at different amplitudes and speeds, and in the next section, the asymmetric hysteresis loops obtained from the tests are modeled by applying some improvements in the Iwan model.

2. Dynamic identification test

The friction between the rope and spring provides the damping required for converting the kinetic energy into thermal energy and reducing the vibration amplitudes in the neighborhood of the resonance frequency. The polyamide 66 material comprises the rope used in the separator, which has high strength and abrasion resistance in addition to the required flexibility as shown in Figure 1 In the design of vibratory separators, the spring constant is determined based on the suspended mass to achieve the desired natural frequency which is k=5.45 N/mm in this case.

Fig. (1) A rope spring passed through the separator.

It is necessary to perform an identification test for a rope spring and record its force response to identify the vibratory separator behavior. Then, the optimal parameters of the model are achieved to match the model results with those from the test by choosing an appropriate physical model and, if necessary, developing it. Different test arrangements were designed and implemented to measure the force of a rope spring in terms of displacement at different amplitudes and frequencies of shaker excitation. The best results were obtained by direct force measurement with the arrangement represented in Figure 2. In order to obtain the force of the spring rope, the spring must be in tension so the spring rope is fixed on one end and a mass is placed at the other end of the spring rope. This mass is connected to the force sensor and finally to the shaker. The force measured in the sensor is named the force after preload, in all figures.

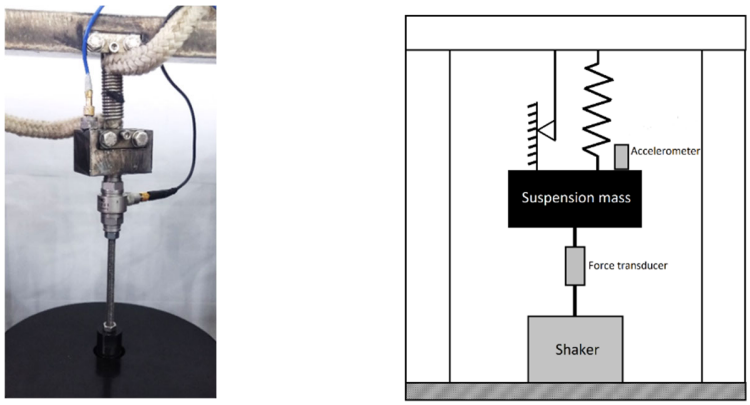

Fig. (2) The vibration test arrangement of a rope spring through direct force measurement.

In the proposed approach, the optimal quality was achieved in the hysteresis curves using an accurate mini shaker (B&K Type 4810) without applying preload to the shaker and using an accelerometer sensor with appropriate sensitivity (YMC 152A100G 105 mv/g) and a force transducer (YMC 512F01 9.55 mV/N), which are represented in Figure 3(a). A NI DAQ USB-4431 dynamic signal acquisition device was used to condition the measured data. Figure 3(b) shows the hysteresis curves after canceling out the linear portion of spring force.

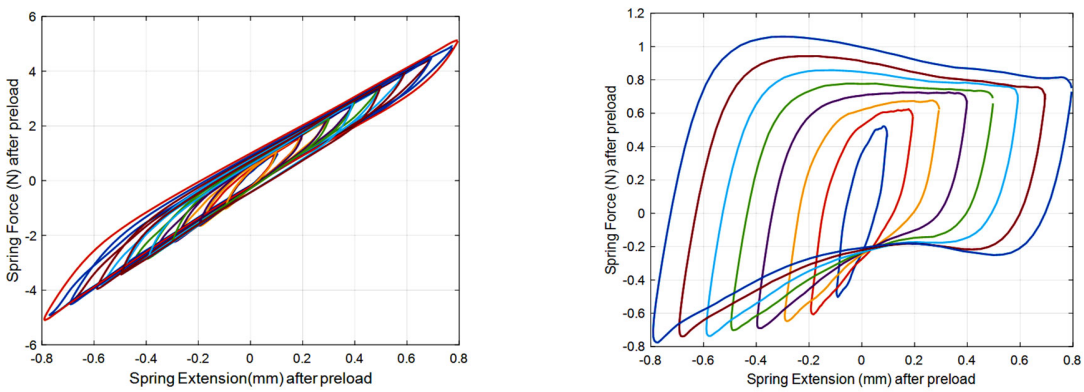

(a) (b)

Fig. (3) The hysteresis loops obtained from the test; **a**. The total spring force, **b**. The spring force without linear portion.

Asymmetry of the hysteresis loop is evident in the path went (upper half of the loop) with the path back (bottom half of the loop), indicating the changed vertical force on the frictional contact surface per oscillation of the separator. In order to examine the effect of slip speed on the friction force, the hysteresis loop diagram is plotted at the same oscillation amplitude and different stimulation frequencies in Figure 4 after canceling out the linear portion of the spring force.

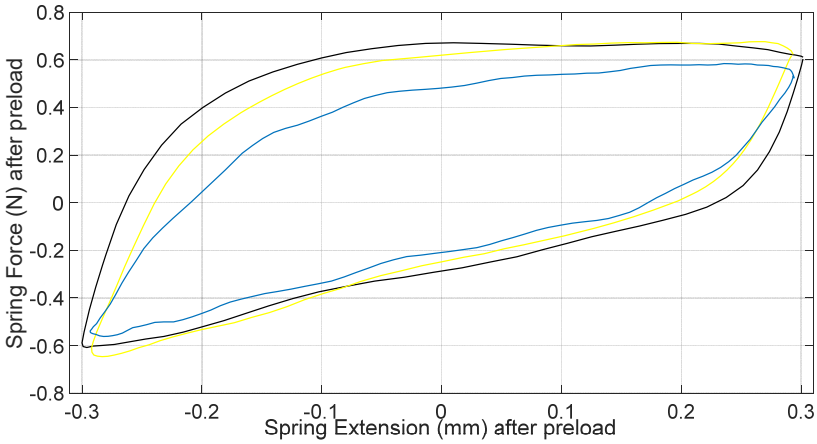

Fig. (4) The hysteresis loop diagram at the same oscillation amplitude and different stimulation frequencies; Blue: *10 Hz*, Yellow: *15 Hz*, black: *20 Hz*.

As shown in Figure 4, the area under the hysteresis curve slightly increases by increasing the stimulation frequency at the same oscillation amplitude, which indicates that the energy absorbed in each cycle also depends on the slip speed, and it is best to consider the effect of slip speed on the friction force in the Iwan model. This phenomenon can be due to the viscoelastic material of the polymer rope and its changed compression rate along with the changed spring length.

3. Model selection

Considering the advantages and disadvantages of different models, the Iwan model was selected for modeling the behavior of the study rope spring. This selection is mainly due to the high flexibility in the Iwan model to reproduce the hysteresis diagrams and the physical interpretation of its parameters which are the advantages of this model.

The Iwan model consists of parallel Jenkins elements each with a linear spring with a stiffness constant of Ki connected in series with a coulomb friction damper. The maximum force tolerated by each friction damper and the damper slips at that force equals to $\tilde{\phi}_i$ with a total element number of N. Consequently, each element is an ideal elastoplastic unit. The total force-displacement hysteresis diagram is shown in Figure. 5 [3].

At first, when the system is subjected to tension, all the springs are active with the maximum stiffness. As the force increases, the force of some springs gradually reaches the limit of friction release, and the other end of the springs slips in the place of the friction damper. Since the springs displace without changing the length, they cannot save great energy, and thus, the total stiffness is reduced. Finally, all the springs reactivate (the maximum stiffness) by changing the force direction and begin to compress until the compression force in some springs reaches the limit of friction release, and again the total stiffness gradually reduces.

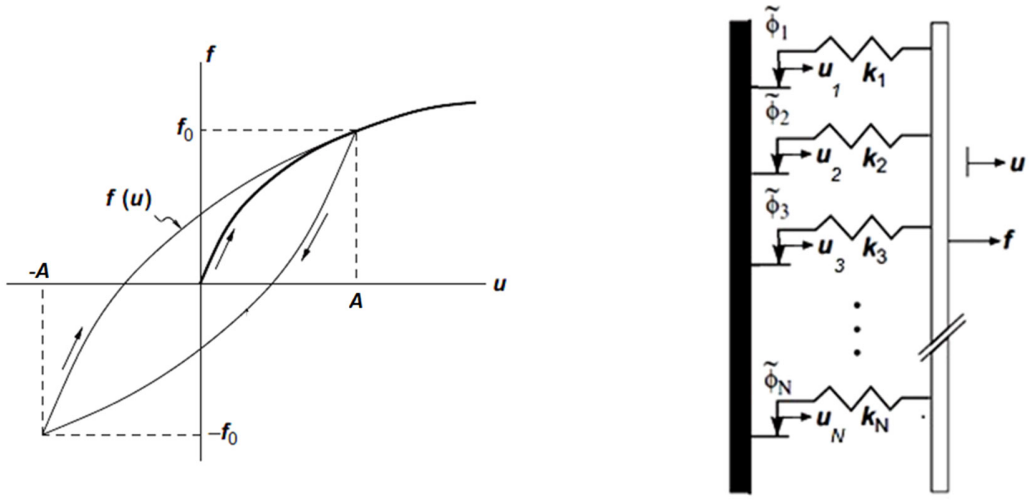

Fig. (5) Schematic diagram of the Iwan model and its hysteresis loop.

The force-displacement relationship for a set of Jenkins elements is defined as follows:

$$f = \sum_{\tilde{\phi}_i \le k_i u} \tilde{\phi}_i + \sum_{\tilde{\phi}_i \ge k_i u} k_i u \tag{1}$$

where the first sigma indicates all the slipped elements and the second sigma indicates the elements remained elastic. Without losing the generality of the model, it can be assumed that all the springs have the same stiffness constant k. Thus, the key parameters that must be identified in the Iwan model are the spring stiffness and the release force in each friction damper.

3.1 . The generalized Iwan model

As shown in the hysteresis diagrams of Figure. 3, the force behavior of the rope spring is different in the round-trip path of the hysteresis loop. Thus, the basic Iwan model that is symmetric needs to be modified to consider the asymmetry of the hysteresis loop and define a model according to the experimental results. Besides, the effect of displacement speed has not been considered in the Iwan model, which needs to be included.

Rajaei included the effect of vertical force variations on the friction surface in the model by applying some improvements to the Iwan model [12]. The generalized Iwan model is actually a generalization of the classic model of the Iwan, which can introduce changes in the normal force on the set of springs and damping of the Jenkins element. The asymmetric hysteresis loops obtained from tests can be modeled through this improved model and by applying the asymmetric vertical force to the round-trip path. In fact, the release force per element $\tilde{\phi}_i$is not constant in this model and has a direct relationship with a vertical force defined as a function of the spring stretching u:

$$F_f(u,\dot{u}) = \frac{k}{k_0} F_f(u_0) + \left(\alpha + \frac{k}{k_0}\alpha_0\right) \int_0^{\frac{kk_0}{k\alpha_0 + k_0\alpha}(u-u_0)} f^* \tilde{\varphi}(f^*) df^* - k(u-u_0) \int_{\frac{kk_0}{k\alpha_0 + k_0\alpha}(u-u_0)}^{\infty} \tilde{\varphi}(f^*) df^* \tag{2}$$

Where $(\ )_0$ indicates the values of the parameter at the path back point, and α indicates the relative variations in the normal force.

Since the force of a simple spiral spring is linear relative to its spring stretching, the linear spring k_p is parallel with a defined set of Jenkins elements as shown in Figure 6.

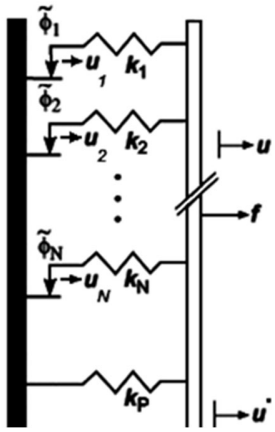

Fig. (6) Schematic figure of the adjusted Iwan model [18].

The rope spring force is defined as the sum of the friction forces between the spring F_f and parallel spring F_P:

$$F(u,\dot{u}) = F_f(u,\dot{u}) + F_p(u) = \frac{k}{k_0}F_f(u_0) - \left(\alpha + \frac{k}{k_0}\alpha_0\right)\int_0^{\frac{kk_0}{k\alpha_0+k_0\alpha}(u-u_0)} f^*\tilde{\varphi}(f^*)\,df^* - k(u-u_0)\int_{\frac{kk_0}{k\alpha_0+k_0\alpha}(u-u_0)}^{\infty}\tilde{\varphi}(f^*)\,df^* + K_p u \tag{3}$$

3.2 . Normal face

In the curves produced in the Iwan model with any arbitrary distribution function, the maximum slope belongs to the points where the movement direction changes. Therefore, the curve gradient should be reduced or constant by moving away from those points. Figure 7 represents the hysteresis curve at the frequency of 15 Hz. In curve abc, the slope is descending from point a to point b and then is negative toward point c. However, in the curve cda, after the initial reduction, the slope of the curve is ascending from point d onwards. This is because of variations in the normal force between the rope and the spring.

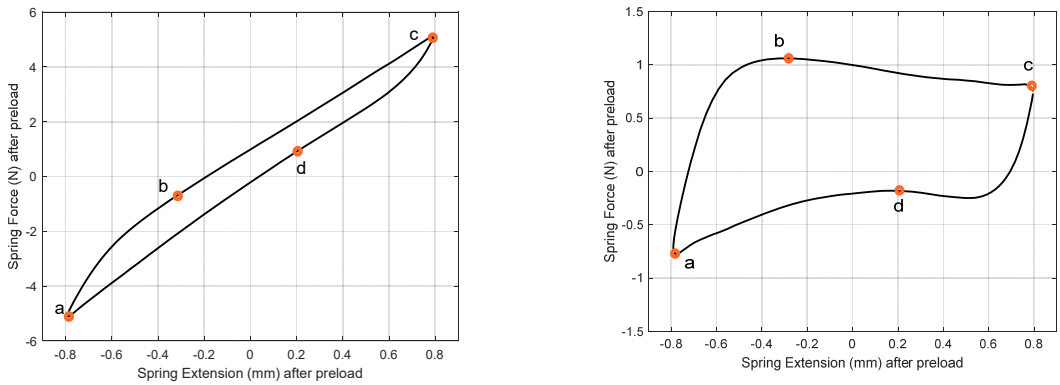

(a) (b)

Fig. (7) The hysteresis curve at the frequency of 15 Hz. **a**. The total spring force, **b**. The spring force without linear portion.

The variations in the normal force are due to stretching/compressing the rope during the spring oscillation. This means that in the rope spring, when the spring reaches the maximum stretching of the rope, the diameter of the rope reduces, and consequently, the normal force between the rope and spring reduces. On the other side, when the spring reaches its minimum length, the normal force increases by compressing and increasing the rope diameter. Different models have been developed to model the normal force. The Hunt and Crossley model is the most widely used one [19] that has been developed based on the Hertz contact model and expresses the contact normal force as follows:

$$N(y,\dot{y}) = k_n y^{\beta} + \lambda k_n y^{\beta} \dot{y} \tag{4}$$

Where y indicates the penetration depth, k_n indicates the nonlinear resilience, λ indicates the nonlinear damping coefficient, and β indicates the power of nonlinear expressions. Since it is assumed that the rope-spring connection force is never zero and also in the preload case, the contact normal force is $\bar{N}$ and y_0 is penetration depth, Equation (4) is rewritten as follows:

$$N(y,\dot{y}) = k_n\left(y^{\beta} - y_0^{\beta}\right) + \lambda k_n y^{\beta} \dot{y} + \bar{N} \tag{5}$$

and the relative variation in the normal force is defined as follows:

$$\alpha(y,\dot{y}) = \frac{N(y,\dot{y})}{\bar{N}} = \frac{k_n\left(y^{\beta} - y_0^{\beta}\right) + \lambda k_n y^{\beta} \dot{y} + \bar{N}}{\bar{N}} + 1 = \tilde{k}_n\left(y^{\beta} - y_0^{\beta}\right) + \lambda \tilde{k}_n y^{\beta} \dot{y} + 1 \tag{6}$$

where $\tilde{k}_n = k_n / \bar{N}$. In Equation (6), if there was no oscillation in-depth, the parameter of relative variations would be equal to unity. The penetration depth defined as rope compression to the inner surface of the spring reaches its minimum at the final spring stretching and its maximum at the final spring compression. Assuming a linear relationship between the penetration depth and displacement:

$$y = \bar{k}\,|A - u| \tag{7}$$

where A indicates the oscillation amplitude and $\bar{k}$ indicates the proportionality constant of two variables, which is assumed to unite in the normal force concerning the coefficient identification.

3.3 . Application of the Iwan model to model the rope spring behavior

It is required to define and optimize a suitable objective function to determine the parameters of the Iwan model for optimal matching of the test results. The objective function is the sum of squared force differences between the points with the same displacement in the test and Iwan model in a complete hysteresis round-trip loop, defined by proper point weighting. The value of this function is always positive, and ideally, i.e., a full agreement between model results and test results is zero.

$$GoalFunction = \frac{1}{(A \times n)} \sum_{(i=1)}^{N} w(i) \times |f_{exp}(i) - f_{model}(i)| \tag{8}$$

$$w(i) = 0.2 + \sqrt{1 - \left(\frac{u_i}{A}\right)^2} \tag{9}$$

where n indicates the total number of measured points in the hysteresis loop, I indicates the number of points in the loop, w(i) indicates the weighting function, f_{exp}(i) indicates the force recorded in the test for the ith point, f_{model} (i) indicates the force calculated from the model for the ith point, and u_i indicates the ith point displacement relative to the center point of the loop. The reason for point weighting concerning the position in calculating the objective function is the compression and aggregation of the measured points at both ends of the hysteresis loop. This is due to the constant sample rate frequency (1280 samples per second) and the minimum speed at both ends of the hysteresis loop. The assumption of the same error weight for all the points in the diagram leads to a good agreement in the end corners of the loop and disagreement in the center points of the loop. Thus, the weighting is done in such a way that more importance is given to the central points of the loop.

In the following, the optimization is done using the genetic algorithm to minimize the objective function. In order to achieve better agreement between the model and test results, different functions were defined for the release force distribution of elements and vertical force on the friction surface, and a comparison was made between the results. For the Iwan distribution function, the best results were achieved by combining three gamma distribution functions. In some references, the uniform or Gaussian distribution function is used [1], in others, functions with a singularity point at the origin are used [20]. The gamma distribution function is the only function that can act similarly to the Gaussian function and also has a singularity point at the beginning of the graph. Employing the set of three gamma functions leads to if the target is a uniform distribution function, it can simulate it with good accuracy. The reason for using three gamma functions is the flexibility of this set in simulating different states:

$$\tilde{\varphi}\left(f^{*}\right)=\sum_{i=1}^{3} g_{i} \frac{f^{*\eta_i-1} \exp\left(-f^{*}/t_{i}\right)}{t_{i}^{\eta_i} \, Gamma\left(\eta_{i}\right)} \tag{10}$$

where η_i and t_i indicate the gamma distribution function parameters and $g_i$indicates the weighting coefficient of each distribution function. The reason for using the gamma distribution function is its flexibility, which can only produce strictly decreasing functions or bell-shaped functions. Based on the results from polynomial functions with different degrees, the relation for vertical force on the friction surface in terms of spring stretching is defined as follows:

$$\alpha\left(u,\dot{u}\right)=\tilde{k}_{n}\left(\left|A-u\right|^{\beta}-A^{\beta}\right)+\lambda\tilde{k}_{n}\left|A-u\right|^{\beta}\left|\dot{u}\right| sign\left(A-u\right)+1 \tag{11}$$

The theoretical and experimental studies show that slip stiffness depends on the contact surface and normal force [21]. According to the experimental observations, the relationship between normal force and stiffness is defined as an exponential function:

Table. (1) The parameters of the Iwan model.

Parameter	Parameter explanation	Parameter unit	The obtained optimal value
k_i	$k\left(\alpha\right)=k_{u}\left(1-\exp\left(-k_{i}\,\alpha/k_{u}\right)\right)$	N/mm	19.62
k_u		N/mm	30.37
$\left[t_1,\eta_1,g_1\right]$	Distribution function coefficients $\tilde{\varphi}\left(f^{*}\right)=\sum_{i=1}^{3} g_{i} \frac{f^{*\eta_i-1} \exp\left(-f^{*}/t_{i}\right)}{t_{i}^{\eta_i} \, Gamma\left(\eta_{i}\right)}.$	-	$\left[0.24,0.95,0.41\right]$
$\left[t_2,\eta_2,g_2\right]$			$\left[0.36,5.1,0.53\right]$
$\left[t_3,\eta_3,g_3\right]$			$\left[0.50,4.4,0.06\right]$
$\tilde{k}_n$	Coefficients of the relative force function normal to the contact surface $\alpha\left(u,\dot{u}\right)=\tilde{k}_{n}\left(\left\|A-u\right\|^{\beta}-A^{\beta}\right)+\lambda\tilde{k}_{n}\left\|A-u\right\|^{\beta}\left\|\dot{u}\right\| sign\left(A-u\right)+1$	1/mm	1.79
λ		-	1.58
β		-	0.0062
Kp	Linear spring stiffness coefficient parallel to the Iwan	N/mm	5.49

$$k\left(\alpha\right)=k_{u}\left(1-\exp\left(-k_{i}\,\alpha/k_{u}\right)\right) \tag{12}$$

where k_i indicates the initial slope of the curve and k_u indicates the final stiffness. Based on the equations above, nine parameters were identified as listed in Table 1, and the optimal values

were obtained for the study separator sample by optimizing the parameters using the genetics algorithm.

Based on the parameters given in Table 1, the diagram for Iwan distribution and relative variations in the normal force are shown in Figures 8 to 10:

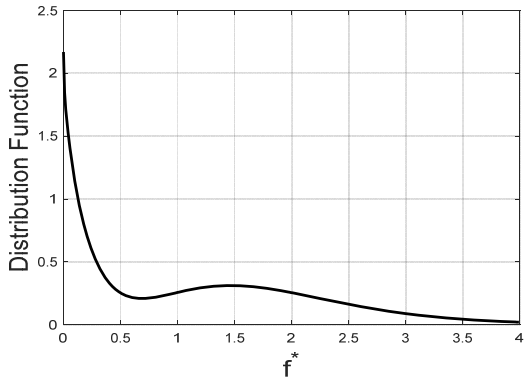

Fig. (8) The Iwan distribution function**.**

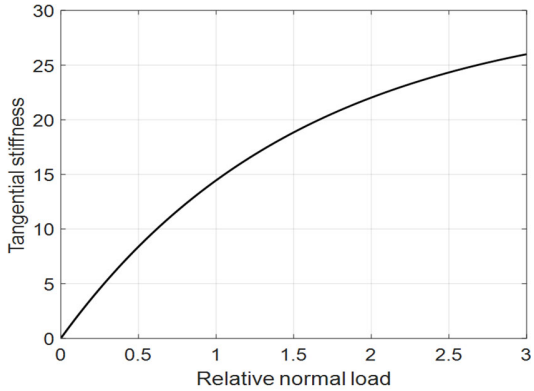

Fig. (9) Iwan stiffness diagram in terms of relative normal force.

According to Figure 10, the vertical force is reduced by increasing the spring stretching. Based on the polymer rope deformation during the spring stretching, it can be found that as the distance between spring rings increases, a bulge is created at the polymer rope compressed by spring rings, and more contact area is created with the spring rings, in total, the normal force increases.

In Figure 11, the diagrams from the test and model are plotted using the parameter values, which represent acceptable agreement for modeling the behavior of friction vibratory separator:

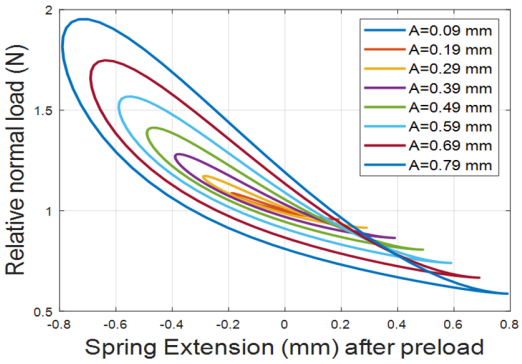

Fig. (10) changes in relative normal force in terms of spring displacement

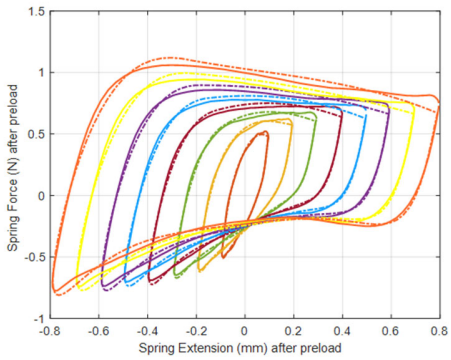

Fig. (11) Force hysteresis diagram in terms of spring displacement from test (stretched line) and model (dashed line)

The classical Iwan model estimates the output force solely on the basis of the relative displacement of the surfaces and is not affected by speed or frequency. As shown in Figure. 4, there is some deviation between the different excitation frequencies in the hysteresis diagram. In

the model employed in this research, the normal force in Equation 11 depends on the speed, so the speed will affect the output of the model. Figure. 12 shows the model prediction at three different frequencies.

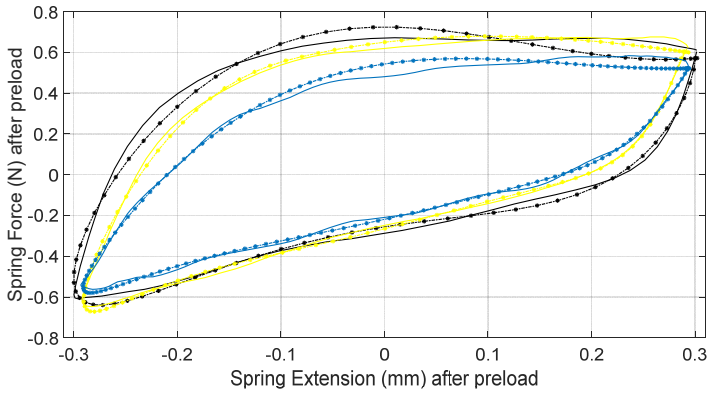

Fig. (12) The hysteresis loop diagram at the same oscillation amplitude and different stimulation frequencies from the test (stretched line) and model (dashed line); Blue: 10 Hz, Yellow: 15 Hz, black: 20 Hz.

4. Conclusion

The dynamic characteristics of a separator with frictional contact are investigated. The Iwan model is used as a natural candidate for contact modeling. This model is generalized for cases where the variation of the normal load has a significant effect on restoring force of contact. Based on observed results, variable normal force affects the obtained hysteresis loops. The modified Hunt and Crossley model is employed to predict the normal force which could capture the frequency dependence of contact behavior.

It can be concluded that by applying the addressed improvements, the Iwan model can be used to model the behavior of microslip and macroslip friction forces with normal force variations and asymmetric hysteresis loop.

References

[1] W.D. Iwan, A distributed-element model for hysteresis and its steady-state dynamic response, (1966).

[2] W.D. Iwan, On a class of models for the yielding behavior of continuous and composite systems, (1967).

[3] R. Bouc, Modèle mathématique d'hystérésis, Acustica, 21 (1971) 16-25.

[4] Y.-K. Wen, Method for random vibration of hysteretic systems, Journal of the engineering mechanics division, 102 (1976) 249-263.

[5] H. Nijmeijer, R. Fey, J. van Aanhold, M. Hulsen, H. Nijmeijer, Modelling and identification of dynamic behaviour of a wire rope spring, Technische Universiteit Eindhoven, Eindhoven, (2004).

[6] S. Rashidi, S. Ziaei-Rad, Experimental and numerical vibration analysis of wire rope isolators under quasi-static and dynamic loadings, Engineering Structures, 148 (2017) 328-339.

[7] M. Leblouba, M. Rahman, S. Barakat, Behavior of polycal wire rope isolators subjected to large lateral deformations, Engineering Structures, 191 (2019) 117-128.

[8] G.F. Demetriades, M.C. Constantinou, A.M. Reinhorn, Study of wire rope systems for seismic protection of equipment in buildings, Engineering structures, 15 (1993) 321-334.

[9] Y. Ni, C. Wong, J. Ko, Modeling the Unsymmetric Hysteretic Loops of Friction-Type Isolators, in: Proceedings of the 14th International Modal Analysis Conference, 1996, pp. 1579.

[10] R. Leenen, The modelling and identification of an hysteretic system, Department of Mechanical Engineering. Eindhoven University of Technology, (2002).

[11] F. Tyan, S.-H. Tu, J. Wu, An Investigation on Mathematical Models of Wire Rope Isolators, in: The 30th National Conference on Theoretical and Applied Mechanics, 2006.

[12] M. Rajaei, H. Ahmadian, Development of generalized Iwan model to simulate frictional contacts with variable normal loads, Applied Mathematical Modelling, 38 (2014) 4006-4018.

[13] H. Ahmadian, M. Rajaei, Identification of Iwan distribution density function in frictional contacts, Journal of Sound and Vibration, 333 (2014) 3382-3393.

[14] J. Mens, A. De Gee, Friction and wear behaviour of 18 polymers in contact with steel in environments of air and water, Wear, 149 (1991) 255-268.

[15] N. Myshkin, M. Petrokovets, A. Kovalev, Tribology of polymers: Adhesion, friction, wear, and mass-transfer, Tribology International, 38 (2005) 910-921.

[16] V. Rodriguez Fereira, J. Sukumaran, P. De Baets, W. Ost, Y. Perez Delgado, M. Andó, Friction and wear properties of polyamides filled with molybdenum disulphide (MoS_2), Mechanical Engineering Letters, 5 (2011) 68-80.

[17] D.M. Nuruzzaman, M.A. Chowdhury, Friction Coefficient of Polymer and Composite Materials Sliding against Stainless Steel, Advanced Materials Research, 576 (2012) 590-593.

[18] Y. Song, C. Hartwigsen, D. McFarland, A.F. Vakakis, L. Bergman, Simulation of dynamics of beam structures with bolted joints using adjusted Iwan beam elements, Journal of sound and vibration, 273 (2004) 249-276.

[19] K.H. Hunt, F.R.E. Crossley, Coefficient of restitution interpreted as damping in vibroimpact, (1975).

[20] D.J. Segalman, A four-parameter Iwan model for lap-type joints, (2005).

[21] W. Sextro, Dynamical contact problems with friction, Springer, 2007.